

Modeling Surface Roughness Effect in Porous Media: From Pore to Core Scale

Yiteng Li^{1,*}, Xupeng He², Hyung Kwak², and Hussein Hoteit¹

¹Ali I. Al-Naimi Petroleum Engineering Research Center, King Abdullah University of Science and Technology, 23955 Thuwal, Saudi Arabia

²EXPEC ARC, Saudi Aramco, 34466 Dhahran, Saudi Arabia

Abstract. NMR relaxometry is an important technique to characterize the structure of porous media. Data analysts very often overlook the surface roughness effect on NMR T2 relaxation and thereby underestimate the pore size distribution. To characterize the surface roughness, we developed an image-based 3D pore surface roughness characterization method by decomposing the connected pore structure into segmented pores with moderate geometry and simple connectivity. Although the surface roughness effect on NMR T2 relaxation has been modeled numerically using the random walk simulation at individual pores, it unambiguously becomes computationally costly with the size of digital rocks increasing, given that the surface relaxation in segmented pore structures must be corrected individually with a unique factor to correct the local surface roughness. To tackle this issue, in this study the surface roughness upscaling problem is transformed to a clustering problem and solved by the evolutionary clustering algorithm. Numerical results show that the proposed data-driven upscaling method yields surface roughness coefficients at the core level that can be used to effectively control the accelerated surface relaxation during the random walk simulation with simple preprocessing.

1. Introduction

NMR relaxometry is an important technique to characterize the structure of porous media [1], as T2 relaxation times are indicative of pore structure if the surface relaxation resides in the fast diffusion limit [2]. When estimating pore sizes from NMR T2 relaxation time, the conventional approach assumes idealized pore shapes with smooth surfaces, and surface relaxivity is viewed as an adjustable parameter to match up with some reference measurements. Furthermore, this analytical model neglects the influence of irregular pore shapes and surface roughness on NMR T2 relaxation, often resulting in underestimated pore sizes [3-6]. To accurately characterize pore structures using NMR relaxometry, it is imperative to consider these geometric effects, necessitating practical techniques for characterizing pore shape irregularities and surface roughness in 3D space.

Despite of this, surface roughness is usually measured in the laboratory using sophisticated microscopy techniques like atomic force microscopy and laser scanner confocal microscopy [3, 4]. These instruments measure surface roughness along a cross-sectional plane of the rock sample, generating precise measurements once the pore-shape/pore-size influence is filtered out. Nonetheless, these approaches are confined to 2D planar areas and are incapable of characterizing 3D surface roughness. It is desirable to have a technologically feasible approach to characterize the surface roughness in 3D space. Micro-computed tomography (μ -CT) is a 3D imaging technique to digitalize rock samples into greyscale images that have been extensively used to study petrophysical properties of formation rocks. Although the finite resolution of μ -CT imaging cannot resolve the actual

surface roughness considering the multiscale nature of surface roughness, an image-based 3D surface roughness characterization method was developed to characterize the “visible” roughness originating from the surface textures at the given resolution [7]. This technology is not limited to the μ -CT imaging; it can produce precise measurement as the resolution of imaging technique increases.

The image-based 3D surface roughness characterization technique includes three main steps. The first step is to decompose the connected pore space into disconnected pore bodies, as the pore structure is too complex to be handled by any shape descriptor. Thus, the subnetwork of over-segmented watershed (SNOW) algorithm is applied to segment pores with effective control of over-segmenting issue [8]. Then a skeleton breakup algorithm is utilized to adaptively simplify the pore structures if necessary. In the second step, the surface of segmented pore structure will be reproduced by the spherical harmonic (SH) functions, yielding a set of SH coefficients [9, 10]. To characterize the surface roughness, it is necessary to define the reference surface that retain the overall shape but excludes the surface textures as much as possible. A subset of SH coefficients is used to build the reference surface such that the enclosed volume of the reference surface has the same volume of the original pore geometry and meanwhile preserves a close pore morphology. The surface roughness is then calculated by making full use of the surrounding vertex information.

The above pore surface roughness characterization method could measure surface roughness of pores partitioned from a digital rock. The effect of surface roughness on NMR

* Corresponding author: yiteng.li@kaust.edu.sa

T2 relaxation is numerically modeled at the pore level using the random walk simulation [11-13]. When extending to digital rocks, we have to apply a unique correction as a function of surface roughness at each individual pore to effectively control the surface relaxation in digital rocks. This significantly increases the computational complexity. Thus, in this study we developed a data-driven upscaling scheme by transforming the original upscaling problem to a clustering problem. Four different clustering algorithms are investigated, including k-means clustering [14], DBSCAN clustering [15], local gravitation clustering [16], and evolutionary clustering [17]. The clustering results are benchmarked to the result obtained by physical partitioning in terms of pore size analysis. The upscaled surface roughness coefficient is then computed from the centroid of each cluster, which will be used to calculate the roughness correction factor. Numerical examples demonstrate that, with some simple modifications, the upscaled surface roughness coefficients can be used to effectively control the surface relaxation. The pore size distribution estimated from the corrected NMR T2 relaxation time could accurately represent the pore structure, which are agree with the results obtained from pore network modeling.

The structure of this paper is organized as follows. In Section 2, detailed procedures are presented to characterize the 3D surface roughness of pores partitioned from a segmented rock image. Then, to expedite surface roughness upscaling, the original problem is transformed to a clustering problem. Four clustering algorithms are investigated in this study, including k-means clustering, density-based spatial clustering of applications with noise (DBSCAN), local gravity clustering, and evolutionary clustering. The upscaled surface roughness coefficients are then to correct surface relaxation during the random walk simulation. Concluding remarks are made at the end, c.

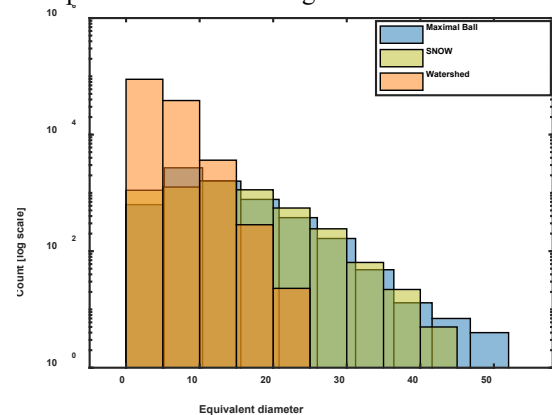
2. 3D pore surface roughness characterization

The irregular pore shape and complex pore connectivity raise enormous challenges in describing the morphology of the pore space using a single mathematical model. To develop an image-based surface roughness characterization technique, it is necessary to simplify the pore structure of a segmented rock image to objects that are readily modeled. Therefore, the key to the success of the technique used in this study is to partition the connected pore space into a plurality of disconnected pore bodies with moderately complex geometry and simple connectivity. Once ready, the surface of the segmented pore geometry is modeled by the spherical harmonic (SH) functions, which are used to build a reference surface from which the surface roughness is defined and parameterized. We will detail each step in the following of this section.

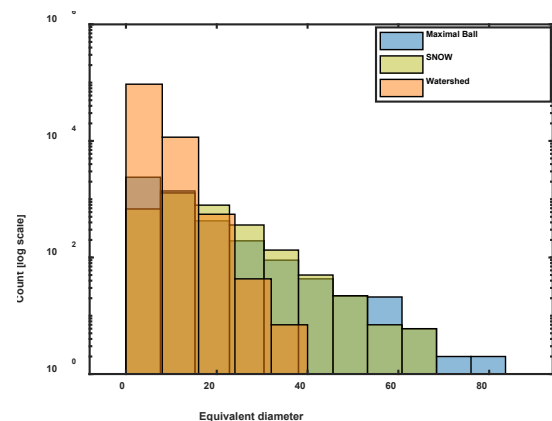
2.1. Pore separation and diagnosis

As highlighted before, the pore space is too complicated to be modeled by a single shape descriptor; thereby it is of vital

importance to apply a proper pore segmentation algorithm, which serves as the cornerstone of subsequent steps [7]. The class of watershed segmentation methods has been extensively used to segment either solid grains or pores for the analysis of grain morphology or the investigation of pore connectivity [8, 18, 19]. In general, watershed segmentation methods compute a distance map where each object of interest has the largest distance that are viewed as the “peak” within a finite region. The peaks are then utilized as markers, regardless of their magnitudes, to determine the “catchment basins” of the binarized rock image, leading to an over-segmentation of the pore space. To reduce the misidentified peaks, Gostick proposed the subnetwork of the over-segmented watershed (SNOW) algorithm [8]. The SNOW algorithm progressively reduces the number of local peaks by smoothing the image with a Gaussian blur filter, removing peaks on the saddle points and ridges, and merging peaks that are sufficiently close in the distance map. Figure 1 illustrates the over-segmentation issue when using a typical watershed segmentation method. In contrast, pore size distributions generated by the SNOW algorithm is consistent with the results of pore network modeling.



(a)



(b)

Fig. 1. Comparison of pore size distributions extracted by a typical watershed segmentation, SNOW, and pore network modeling for (a) sandstone (b) carbonate ¹.

¹ The rock samples are downloaded from <https://www.imperial.ac.uk/earth-science/research/research-groups/pore-scale-modelling/micro-ct-images-and-networks>.

Figure 2 shows the pore structures partitioned from the Berea sandstone as shown in Figure 1(a). We randomly color the pores for illustration purposes only. It is worth noting that the original tiny pore throats may become twig-shaped corners on the surface of segmented pores. These sharp textures increase the failure of the proposed surface roughness characterization method. To increase the robustness and reliability, the generated pore surface is first slightly eroded, then followed by a dilation operation, to remove such surface textures. Although many of the generated pore bodies can be easily handled using SH, some of them may still retain complex geometry. To continue simplifying these pore structures, the skeleton breakup algorithm is developed to cut off the skeleton of the voxelized pore structure in a hierarchical manner. Figure 3 shows the skeleton of a segmented pore by the image thinning operation until the medial axis of the resultant structure remains a unit voxel length. The bridging nodes (shown in red), which are comprised of one to multiple voxels, connect the links between them that constitute the skeleton backbone. The skeleton breakup algorithm first calculates the connectivity of bridging nodes along the backbone. Depending on the pore size and complexity, it either removes the most “busy” node that connects the highest number of links, or the longest link on the backbone connecting to it. Then the remaining structure will be used as markers to perform the watershed segmentation, which ideally divides the object of interest into two constituents with lower complexity. This process continues until the generated pore geometries are considered simple enough that cannot be split. In addition, to avoid over-segmentation, the skeleton breakup is terminated if the number of pore voxels is smaller than 5000.

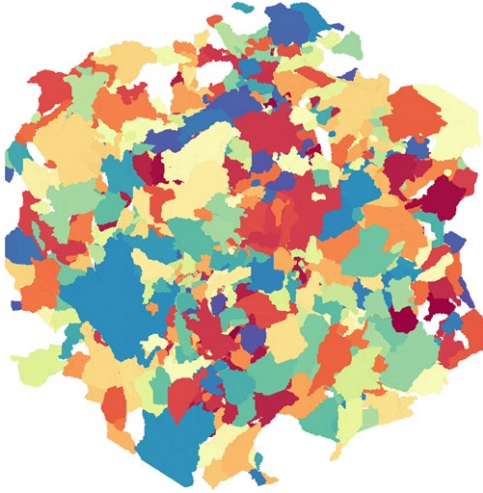


Fig. 2. Illustration of disconnected pore bodies partitioned from the Berea sandstone using the SNOW algorithm. The corresponding pore size distribution is shown in Figure 1(a).

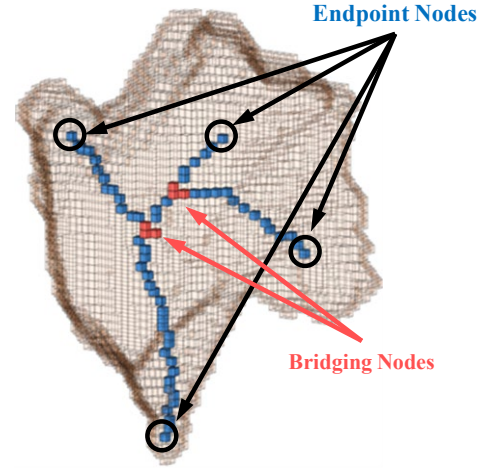


Fig. 3. Skeletonization of a disconnected pore geometry. The red voxels represent the bridging nodes, while the blue voxels represent the links that constitute the skeleton, with the endpoint node marked by black circle.

2.2. Pore surface reconstruction

Once the pore space is well split, each voxelized pore structure is replaced by a triangular surface mesh. This preprocessing would remarkably improve the accuracy, efficiency, and robustness of the surface reconstruction step. Furthermore, we build a bijective mapping between mesh vertices on the pore surface $(x, y, z)^T$ and mesh vertices on the parameter surface $(\theta', \varphi')^T$ of a unit sphere, where θ' and φ' range from $[0, \pi]$ and $[0, 2\pi]$ respectively. The initial parameterization often produces a low-quality mesh, reducing the accuracy and efficiency of surface reconstruction. To improve the parameter mesh quality, the Control of Area and Length Distortion (CALD) algorithm, proposed by Shen and Makedon [9], is applied in this study.

With a proper spherical parameterization as shown in Figure 4, the pore surface can be modeled as follows

$$x(\theta', \varphi') = \sum_{n=0}^N \sum_{m=-n}^n c_{x_n}^m Y_n^m(\theta', \varphi') \quad (1)$$

$$y(\theta', \varphi') = \sum_{n=0}^N \sum_{m=-n}^n c_{y_n}^m Y_n^m(\theta', \varphi') \quad (2)$$

$$z(\theta', \varphi') = \sum_{n=0}^N \sum_{m=-n}^n c_{z_n}^m Y_n^m(\theta', \varphi') \quad (3)$$

where θ' and φ' are the polar coordinates of vertices on the parameter surface. The real form of the SH function $Y_n^m(\theta', \varphi')$ is given by

$$Y_n^m(\theta', \varphi') = \sqrt{\frac{(2n+1)(n-m)!}{4\pi(n+m)!}} P_n^m(\cos \theta') \cos(m\varphi'), m \geq 0 \quad (4)$$

$$Y_n^m(\theta', \varphi') = \sqrt{\frac{(2n+1)(n-|m|)!}{4\pi(n+|m|)!}} P_n^{|m|}(\cos \theta') \sin(|m|\varphi'), m < 0 \quad (5)$$

with the associate Legendre function P_n^m being

$$P_n^m = (-1)^m (1-x^2) \frac{d^m}{dx^m} \left[\frac{1}{2^n n!} \frac{d^n}{dx^n} (x^2-1)^n \right]. \quad (6)$$

In the above formulations, n is the index of the SH degree, and N is the maximum degree of spherical harmonics. From Figure 5, as N increases, more detailed surface textures can be reproduced. The SH coefficients $c_{x_n}^m$, $c_{y_n}^m$, and $c_{z_n}^m$ are solved by the standard least squares algorithm, given that the number of equations is often greater than the number of SH coefficients. In this study, the maximum degree of spherical harmonics is set to 40.

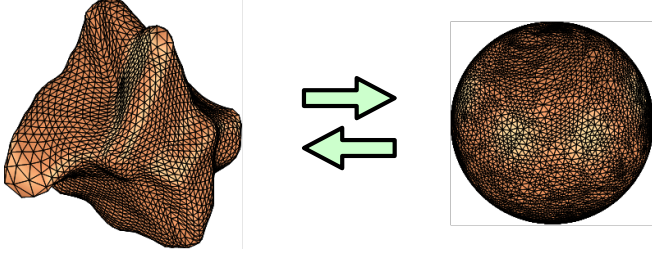


Fig. 4. Bijective mapping between the pore surface and the parameter surface of a unit sphere using spherical parameterization.

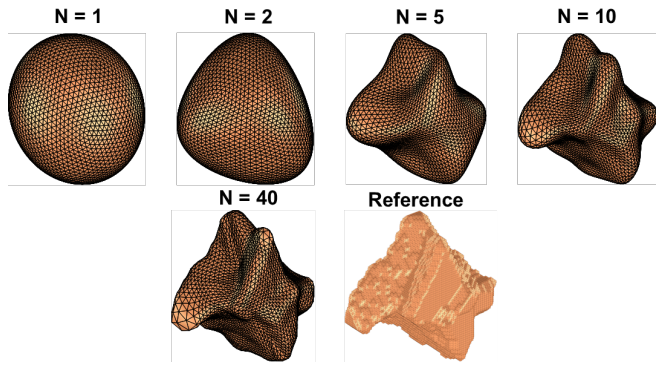


Fig. 5. Pore surface reconstruction as a function of the maximum degree of spherical harmonics. The original voxelized pore structure is shown as the reference.

2.3. Surface roughness parameterization

Characterization of surface roughness often relies on the definition of the reference curve/plane. It is observed from Figure 5 that reducing the total degree of spherical harmonics gradually excludes surface textures from the reconstructed surface. The reference surface is supposed to keep the overall shape but discard local surface textures as much as possible. To determine the optimal N for building the reference surface, the geometry enclosed by the reference surface is required to have the same volume, as well as similar elongation and flatness. Numerical experiments show that $N = 6$ yields satisfactory results. Figure 6 shows a voxelized pore structure on the left and the corresponding pore surface reproduced with $N = 40$ on the right. The pore surface is shown in green color with grey lines, while the reference

surface is shown in white color with blue lines), which retains the overall pore shape but excludes many surface textures.

(b)

Fig. 6. Comparison of (a) voxelized pore structure and (b) the reconstructed pore surface and the reference surface.

To parameterize the surface roughness, we first define some necessary parameters, see Figure 7. In the figure, the pore surface is colored in yellow while the reference surface is represented by the white triangulations with black lines. The i th vertex of the reference surface has m surrounding vertices that delineate a region (marked in red) of finite area \hat{a}_i . We denote by h_i the height measured from the reference surface to the pore surface along the vertex normal direction. If $h_i > 0$, it indicates the pore surface extrudes from the reference surface; instead, the pore surface intrudes into the reference surface with $h_i < 0$. The distance between the vertex i and vertex j is denoted by Δx_j ($j = 1, \dots, m$).

Then the local roughness at vertex i is defined as

$$r_i = \left(\prod_{j=1}^m \frac{dh_{ij}}{dx_{ij}} \right)^{\frac{1}{m}} = \left(\prod_{j=1}^m \frac{|h_j - h_i|}{\Delta x_j} \right)^{\frac{1}{m}} \quad (7)$$

Eq. (7) is the geometric mean of the ratio of the local height difference to the distance between a pair of the pivot and surrounding vertices, which make full use of regional information for surface roughness characterization. With iterating all valid vertices on the reference surface, the (overall) surface roughness is defined by

$$\lambda_k = \frac{\sum_i |r_i| \hat{a}_i}{A}, \quad k=1, \dots, N_p \quad (8)$$

where λ_k is the surface roughness coefficient. A is the sum of the areas of valid surface triangulations that constitute the reference surface. The subscript k denotes the k th pore bodies partitioned from the porous space of the rock.

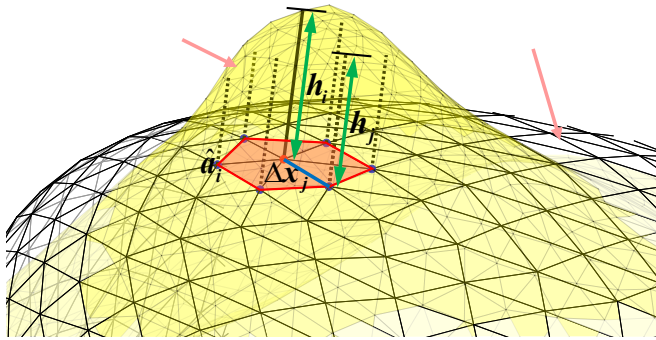


Fig. 7. Schematic diagram of surface roughness parameterization. The pore surface is colored in yellow and the reference surface is represented by white triangulations with black lines. The definitions of \hat{a}_i , h_i , h_j , and Δx_j are described in the context.

3. Upscaling roughness from pore to core scale

Now the surface roughness of segmented pores can be characterized using the method described in Section 2. With hundreds of pores partitioned from a digital rock, a lot of surface roughness coefficients are computed. Naturally, upscaling of pore surface roughness can be transformed to a clustering problem, shown as Figure 8. The upscaled surface roughness coefficient is calculated by the centroids of the clusters. We use this value to represent the surface roughness coefficient of the pores in the same cluster, which is then used to correct the NMR T2 relaxation computed from random walk simulations in digital rock.

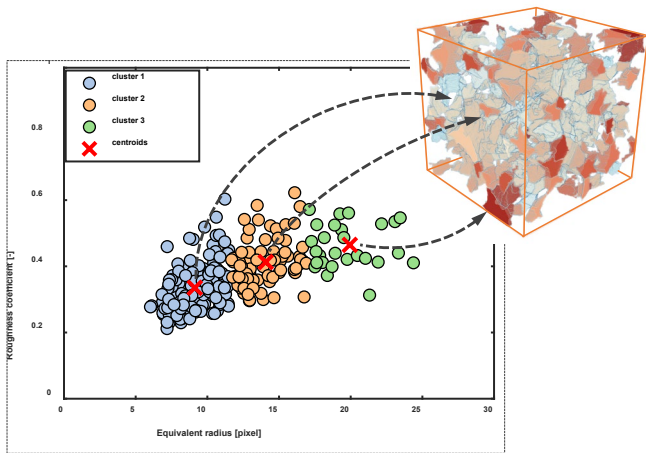
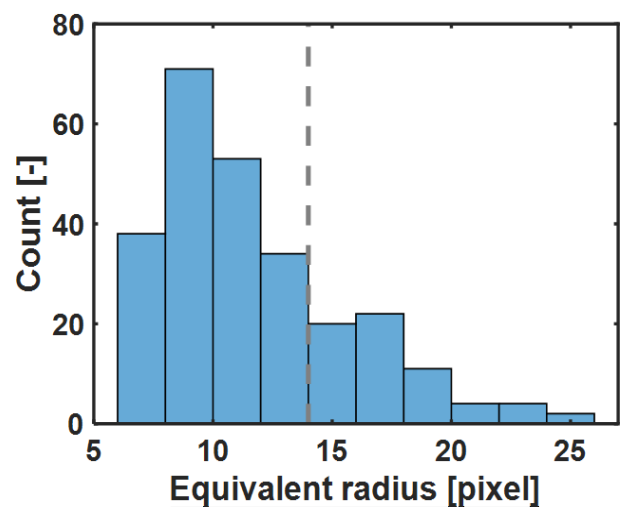


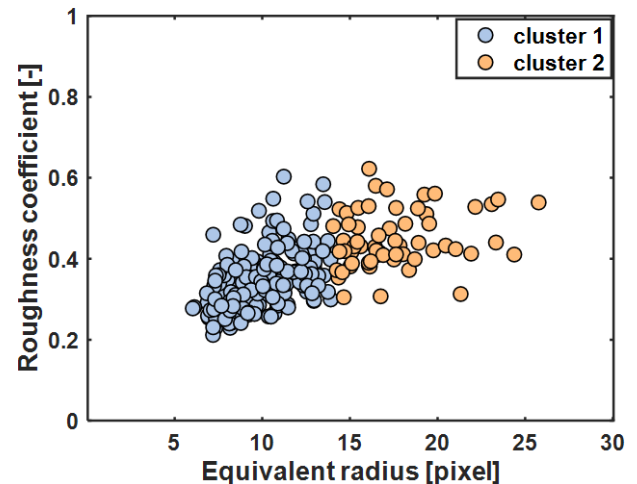
Fig. 8. Schematic diagram of upscaling surface roughness from pore to core scale. The centroid of each cluster yields an upscaled surface roughness coefficient.

In the following, the Berea sandstone, shown in Figure 2, is used to validate the data-driven upscaling method. Four clustering algorithms are investigated, including k-means clustering, DBSCAN clustering, local gravitation clustering, and evolutionary clustering. To evaluate their performances, the results of the four clustering algorithms are benchmarked to the result generated by partitioning the clustered data in terms of the pore size distribution (see Figure 9 (a)). The grey dash line divides the pore size distribution into categories, yielding two clusters as shown in Figure 9 (b). In addition, at each pore size, different surface roughness coefficients are calculated with roughly equal bandwidth. This is in line with

our expectation that the surface roughness is influenced by the morphology of grain surfaces due to the sedimentation and diagenesis process. On the other hand, a weak relationship is observed between the surface roughness coefficient and equivalent pore radius. The equivalent radius is defined as the radius of the spherical pore that honors the same volume as a partitioned pore structure. It intuitively makes sense for the image-based surface roughness characterization method. Under a finite imaging resolution, the pore structure comprised of more void voxels is prone to exhibit more complex surface morphology. It has to be noted that the 3D pore surface roughness characterization method captures the “surface roughness” (surface textures) at a finite length scale. Even though it is not the actual roughness given the multiscale nature of surface roughness, the above observations do not contradict each other.



(a)



(b)

Fig. 9. (a) pore size distribution of the Berea sandstone and (b) partitioning of pore surface roughness coefficients into two clusters.

It is desirable to automatically partition data into different clusters instead of analyzing the distribution of pore sizes or morphology parameters. The selection of the threshold value is subjective and biased, and also highly depends on the experience of data analysts. To tackle this issue, k-means clustering, DBSCAN clustering, local gravity clustering, and

evolutionary clustering are tested for surface roughness upscaling. In particular, k-means clustering, as well as its variants, partitions data into k clusters in which data points belonging to the same cluster share the nearest mean. This class of methods typically demands prior knowledge of the available number of clusters (e.g. the number of pore types in our case), making it less appealing for practical applications. Another method under investigation is the DBSCAN (Density-Based Spatial Clustering of Applications with Noise), which classifies observations into core points, border points, and outliers. Generally, it partitions data in terms of the density of regional data. The distinct advantage of density-based clustering algorithms over k-means clustering is it doesn't need any prior knowledge. A special density-based clustering algorithm, called local gravitation clustering, is applied as well, which treats each data point as an object with mass and associates with the local resultant force generated by its neighbors. This method leverages the difference of the local resultant force of the data points, depending on their locations (either at cluster center or cluster border), to accomplish cluster separation. However, this method requires the number of neighbors as input, and an inappropriate estimate could result into an unsatisfactory result. The last method used in our study is evolutionary clustering in which the clustering problem is reformulated as an optimization problem and solved by the differential evolution algorithm. The surface roughness coefficients are partitioned into different clusters by minimizing the sum of the distance between a data point and the centroid of the cluster it belongs to. Table 1 shows all the required inputs for the four clustering algorithms.

Table 1. Input parameters of four clustering algorithms for surface roughness upscaling.

Algorithm	Inputs	value
k-means clustering	number of clusters	2
DBSCAN clustering	neighborhood scan radius	0.35
	minimum number of neighbors	3
Local gravitation clustering	number of neighbors	40
Evolutionary clustering	number of iterations	200
	Population size	50
	Crossover probability	0.2

Figure 10 shows the results of the aforementioned four clustering algorithms. It is observed that the DBSCAN method, see Figure 10(b), over-partitions the surface roughness coefficients; all the other methods correctly predict the number of clusters, albeit the number of clusters is specified as input for k-means clustering. The accuracy of the other three clustering methods is very close, and evolutionary clustering works slightly better. Although evolutionary clustering has to set three input parameters, these parameters are very typical; instead, the k-means clustering, DBSCAN clustering and local gravitation clustering require some prior knowledge to specify the inputs, which are prone to be case-dependent. Given this, evolutionary clustering provides an

automatic approach to upscale surface roughness from pore scale to core scale.

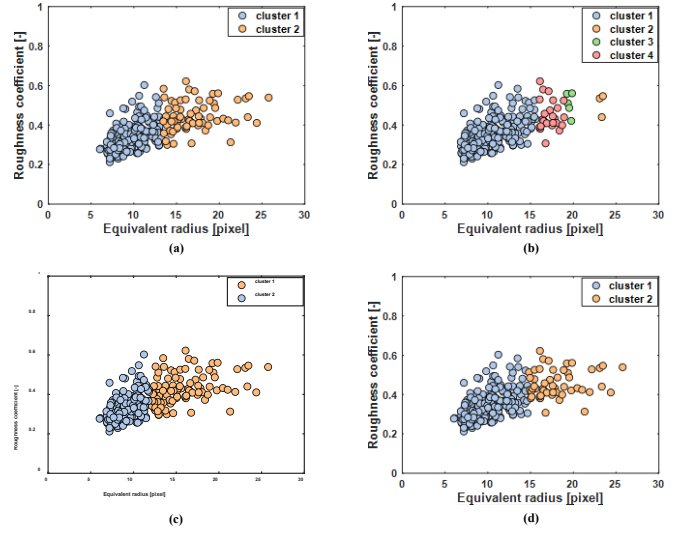


Fig. 10. Partitioning of pore surface roughness coefficients using (a) k-means clustering, (b) DBSCAN clustering, (c) local gravitation clustering, and (d) evolutionary clustering.

The representative surface roughness coefficients calculated from the centroids of the cluster 1 and 2 in Figure 10 (d) are 0.3694 and 0.4536. The presence of surface roughness increases the surface-volume ratio and thereby accelerates the surface relaxation. Without accounting for the surface roughness effect, data analysts would underestimate pore sizes (R) by using the analytical equation shown below [1]

$$R = 3\rho T_2 \quad (9)$$

where ρ is the surface relaxivity [$\mu\text{m/s}$] and T_2 is the transverse relaxation time [s]. The NMR T_2 relaxation can be modeled by the random walk simulation [11-13], which mimics the Brownian motion of nuclear spins (abstracted as particles) in the porous media. The physical process of nuclear magnetization decay due to surface relaxation is simulated by multiplying the nuclear magnetization m with a factor of $(1-p)$ whenever a particle collides with solid grains such that

$$m(t + \Delta t) = m(t) \times (1-p) \quad (10)$$

where

$$p = \frac{2\rho ds}{3D_0} \quad (11)$$

In Eq. (11), ds is the diffusion distance travelled at a time step [μm] and D_0 is the bulk diffusion coefficient [$\mu\text{m}^2/\text{s}$].

To correct the surface roughness effect, we define the roughness correction factor (α), as the inverse of the exponential of the upscaled surface roughness coefficient. The roughness correction factor is then assigned to the solid voxels surrounding the pores. If a particle collides with a solid voxel, it will bounce back and obtain the local roughness

correction factor, reducing p by multiplying $\alpha \leq 1$. Now the Eq. (11) becomes

$$p = \frac{2\rho ds}{3D_0} \times \alpha \quad (12)$$

If the surface roughness coefficient is zero, indicating a smooth surface without roughness, the roughness correction factor is equal to one such that Eq. (12) returns back to Eq. (11). Figure 11 shows the pore size distributions interpreted from Eq. (9). The blue solid line does not account for the surface roughness effect, while the red solid line is obtained with each separated pore having its own roughness correction factor. The black dash line is computed based on the upscaled roughness coefficients. The numerical experiment demonstrates that ignoring the surface roughness effect would underestimate the pore size distribution. In addition, the roughness correction factors, estimated from the upscaled surface roughness coefficients, work well, and the computed results consistent with the result obtained from pore network modeling.

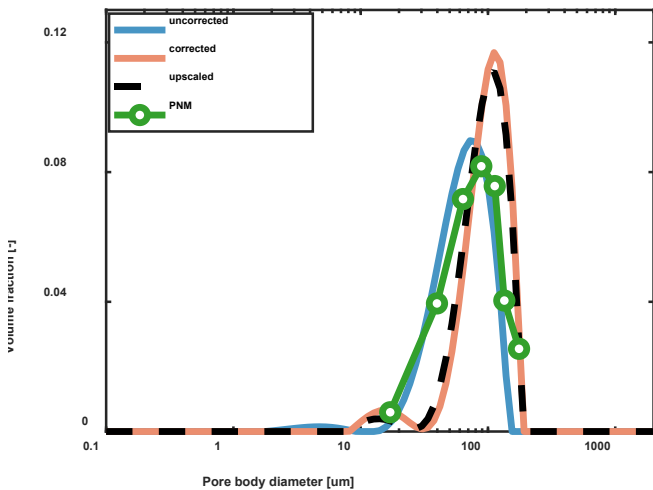


Fig. 11. Pore size distribution of the Berea sandstone interpreted from NMR T2 relaxation time. The green solid line with circles is the result obtained from pore network modeling.

4. Conclusion

In this study, we developed a data-driven pore surface roughness upscaling method and solved the upscaling problem with the evolutionary clustering algorithm. Surface roughness data are generated by an image-based pore surface roughness characterization technique, including pore separation, surface reconstruction, and roughness parameterization. The key to the success of 3D surface roughness characterization relies on decomposing the connected pore space into pores with low to medium morphological complexity and connectivity. Then, we leverage spherical harmonics to reproduce pore surfaces and build the reference surface from which the surface roughness is characterized and parameterized. By comparing four clustering algorithms, evolutionary clustering provides an automatic approach to partition surface roughness coefficients with good accuracy. The upscaled surface roughness coefficients are calculated by evaluating the

centroids of existing clusters. We introduce the roughness correction factor as a function of the surface roughness coefficient to correct the surface roughness effect in random walk simulations. The corrected NMR T2 curves could properly estimate the pore size distribution, consistent with the result from pore network modeling. Future works include extending the proposed method to carbonates and developing a simple and universal formulation to estimate roughness correction factor for both sandstones and carbonates.

Acknowledgments

We would like to thank Saudi Aramco for funding this research. We would also like to thank King Abdullah University of Science and Technology (KAUST) for providing a license for MATLAB.

References

1. G.R. Coates, L. Xiao, M.G. Prammer, *NMR logging: principles and applications*, (1999).
2. K.R. Brownstein, C.E. Tarr, *Phys. Rev. A* **19**, 2446 (1979).
3. S.M. Ma, G. Singer, S. Chen, M. Eid, *SPE J.* **26**, 2860 (2021).
4. G. Singer, S.M. Ma, S. Chen, M. Eid, *2D Surface Roughness Quantification for Enhanced Petrophysical Applications*, (OnePetro, Houston, 2022).
5. Y. Li, X. He, M. AlSinan, E. Ugolkov, H. Kwak, H. Hoteit, *Numerical Study of Surface Roughness Influence on NMR T2 Response*, (EAGE, Madrid, 2022).
6. Y. Li, M. Alsinan, X. He, E. Ugolkov, H. Kwak, H. Hoteit, *NMR T2 Response in Rough Pore Systems: Modeling and Analysis*, (OnePetro, Houston, 2022).
7. Y. Li, X. He, H. Kwak, H. Hoteit, *Advanced Imaged-based Workflow for 3D Pore Surface Roughness Quantification*, (SCA, Abu Dhabi, 2023)
8. J.T. Gostick, *Phys. Rev. E* **96**, 023307 (2017).
9. L. Shen, F. Makedon, *Image Vis. Comput.* **24**, 743 (2006).
10. L. Shen, H. Farid, M.A. McPeck, *Evol.* **63**, 1003 (2009).
11. O. Talabi, S. Alsayari, M.A. Fernø, H. Riskedal, A. Graue, M.J. Blunt, *Pore-scale simulation of NMR response in carbonates*. (SCA, Abu Dhabi, 2008).
12. C.H. Arns, A.P. Sheppard, R.M. Sok, M.A. Knackstedt, *Petrophys.* **48**, (2007).
13. Y. Li, W. Zhu, X. He, H. Kwak, H. Hoteit, *GPU-Accelerated NMR T2 Simulator Incorporating Surface Roughness Effect*, (OnePetro, San Antonio, 2023).
14. J. MacQueen, *Some methods for classification and analysis of multivariate observations*, (1967).
15. M. Ester, H.P. Kriegel, J. Sander, X. Xu, *A density-based algorithm for discovering clusters in large spatial databases with noise*, (1996).
16. Z. Wang, Z. Yu, C. P. Chen, J. You, T. Gu, H. S., Wong, J. Zhang, *IEEE transactions on cybernetics*, **48**, 5 (2017).
17. G. Chen, W. Luo, T. Zhu, *Evolutionary clustering with differential evolution*. *IEEE*, Beijing, (2014).

18. A. Rabbani, S. Jamshidi, S. Salehi, J. Pet. Sci. Eng. **123**, 164 (2014).
19. D. Kong, J. Fonseca, Géotechnique **68**, 249 (2018).